Limnol. Oceanogr., 56(4), 2011, 1355–1371

doi:10.4319/lo.2011.56.4.1355

Methyl mercury dynamics in a tidal wetland quantified using in situ optical measurements

B. A. Bergamaschi,[a,*] J. A. Fleck,[a] B. D. Downing,[a] E. Boss,[b] B. Pellerin,[b] N. K. Ganju,[c] D. H. Schoellhamer,[a] A. A. Byington,[d] W. A. Heim,[d] M. Stephenson,[d] and R. Fujii[a]

[a] United States Geological Survey California Water Science Center, Sacramento, California
[b] University of Maine School of Marine Sciences, Orono, Maine
[c] United States Geological Survey Woods Hole Science Center, Woods Hole, Massachusetts
[d] California Department of Fish and Game Marine Pollution Studies Laboratory, Moss Landing, California

Abstract

We assessed monomethylmercury (MeHg) dynamics in a tidal wetland over three seasons using a novel method that employs a combination of in situ optical measurements as concentration proxies. MeHg concentrations measured over a single spring tide were extended to a concentration time series using in situ optical measurements. Tidal fluxes were calculated using modeled concentrations and bi-directional velocities obtained acoustically. The magnitude of the flux was the result of complex interactions of tides, geomorphic features, particle sorption, and random episodic events such as wind storms and precipitation. Correlation of dissolved organic matter quality measurements with timing of MeHg release suggests that MeHg is produced in areas of fluctuating redox and not limited by buildup of sulfide. The wetland was a net source of MeHg to the estuary in all seasons, with particulate flux being much higher than dissolved flux, even though dissolved concentrations were commonly higher. Estimated total MeHg yields out of the wetland were approximately 2.5 μg m^{-2} yr^{-1}—4–40 times previously published yields—representing a potential loading to the estuary of 80 g yr^{-1}, equivalent to 3% of the river loading. Thus, export from tidal wetlands should be included in mass balance estimates for MeHg loading to estuaries. Also, adequate estimation of loads and the interactions between physical and biogeochemical processes in tidal wetlands might not be possible without long-term, high-frequency in situ measurements.

Mercury accumulation in coastal and estuarine environments poses significant risks to humans and wildlife as methylmercury (MeHg) is concentrated in aquatic food webs. The greatest risk from MeHg exposure is its potent neurotoxicity (Mergler et al. 2007; Selin 2009; Tan et al. 2009). For humans, there is evidence for elevated risk of cardiovascular disease and potential adverse effects on the immune and endocrine systems (Mergler et al. 2007; Tan et al. 2009). In fish and wildlife, Hg accumulation has been associated with neurological and behavioral abnormalities, low reproductive success, and direct toxicity (Mitro et al. 2008; Crump and Trudeau 2009).

Estuaries represent important sites of mercury contamination because of relatively high MeHg concentrations and the abundance of fish and bird populations (Mason et al. 2006; Eagles-Smith and Ackerman 2009). Traditional mass balance studies of MeHg in estuaries typically assess the riverine loads, point sources, and atmospheric deposition, whereas more recent studies also examined the patterns of production, occurrence, and transport of MeHg in estuary sediments (Fitzgerald et al. 2007; Merritt and Amirbahman 2009). These studies found that production of MeHg principally occurs in near-surface sediments, where concentrations can be quite high but also where production might be substantially offset by oxidation within the sediment column (Choe et al. 2004). Consequently, the extent to which MeHg is released from the sedimentary environment and incorporated into estuarine food webs, particularly of piscivorous fish, is controversial (Mason et al. 2006; Benoit et al. 2009).

Fewer studies have examined the extent to which tidal wetlands can supply MeHg to estuaries. Tidal wetland MeHg production has been associated with high organic matter production (Hall et al. 2008), vegetation uptake and decomposition (Windham-Myers et al. 2009), metal cycling (Mitchell and Gilmour 2008), and wetland sediment MeHg production (Heim et al. 2007). Because tidal exchange in estuarine and coastal marshes drives a significant flux of wetland-derived material into surrounding surface waters (Eckard et al. 2007; Hall et al. 2008; Kraus et al. 2008), production of MeHg in tidal marsh systems could be an important source of MeHg to pelagic estuarine food webs. Tidal export from wetlands links the zone of MeHg production to open-water areas (Hall et al. 2008; Mitchell and Gilmour 2008). Once in open waters, MeHg can become preferentially associated with phytoplankton (Gorski et al. 2008) and thereby enter the base of the pelagic piscivorous food web (Mason et al. 2006). However, quantifying the contribution of estuarine wetlands is difficult because the concentration of MeHg varies continuously and the net flux into or out of a tidal wetland is the tidal residual—the difference between the much larger fluxes that occur during each ebb and flood that are driven by tidal flows (Ganju et al. 2005).

The use of in situ optical proxies has been successful in measuring a variety of constituents in dynamic systems for which traditional sampling was insufficient. For example, in situ optical proxies have been used to determine

* Corresponding author: bbergama@usgs.gov

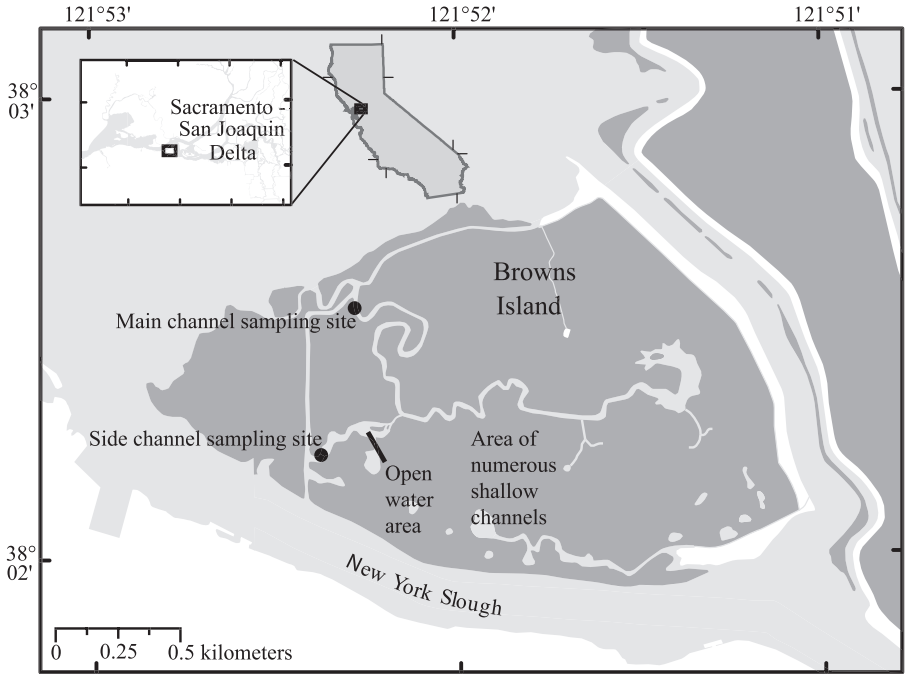

Fig. 1. Map of in situ deployment locations on Browns Island. Inset shows location of Browns Island in San Francisco estuary.

sediment and dissolved fluxes in tidal and nontidal systems (Ganju et al. 2005; Downing et al. 2008), dissolved organic carbon in tidal systems and upstream storm watersheds (Downing et al. 2009; Saraceno et al. 2009), and cycling of organic matter and nutrients (Spencer et al. 2007; Pellerin et al. 2009). Although in situ optical measurements have not previously been used to assess MeHg concentrations, the reported strong relationships with organic material (Fitzgerald et al. 2007; Canario et al. 2008; Selin 2009) and between Hg and lab-based optical measurements (Mitchell and Gilmour 2008; Dittman et al. 2009) suggest the potential of such an approach is high.

The goals of this study were to improve our understanding of the hydrologic, biologic, climatic, and geomorphic properties that affect MeHg exchange in tidal wetland systems and to assess the extent to which tidal advective transport of MeHg from wetlands represents a significant source to estuarine environments. The study was guided by the following hypothetical conceptual model, wherein tidal exchange of dissolved MeHg (DMeHg) is limited by hydrologic connectivity and tidal transport. We hypothesized that because tide heights vary over spring–neap cycles, areas of the wetland distant from the channel are hydrologically decoupled from the main channels for substantial periods of time. Any DMeHg accumulated during the decoupled period would be released as the tidal range increased, going from neap periods to springs (Guentzel 2009). But MeHg production may be suppressed when decoupled because sulfide accumulation can limit methylation rates by reducing availability of Hg(II) (Mitchell and Gilmour 2008) and by inhibiting the sulfate reduction rate (Han et al. 2008). Dissolved organic matter (DOM) could also have an effect; an insufficient supply of labile DOM could limit methylation by limiting microbial activity, whereas binding of Hg(II) to DOM could inhibit methylation (Ravichandran 2004; Merritt and Amirbahman 2009). The DOM concentrations measured at the study site are high, but bioavailability is poor (Stepanauskas et al. 2005; Kraus et al. 2008).

The hypothetical model further posits that the transport of particle-associated MeHg (PMeHg) is largely separate from dissolved transport, with PMeHg accumulating in a sediment repository—either on the marsh plain or in wetland channels—and entrained in response to energetic events, such as high channel velocities or wind–wave resuspension external to the wetland. Entrained particles are then subject to tidal transport.

We are aware of no previously published studies that have quantitatively assessed the flux of MeHg onto or off of tidal wetlands, owing to the difficulty of making flux measurements in tidal systems (Ganju et al. 2005) and the expense of MeHg sampling and analysis. Because of the tremendous emphasis placed on wetland restoration in aquatic recovery schemes, it is important to understand their contribution to estuarine and coastal mercury cycling. As has been suggested for nearshore coastal sediments, habitat and ecosystem improvements could substantially alter MeHg production and transport, potentially increasing mercury concentrations in biota (Hammerschmidt and Fitzgerald 2006).

Methods

Site description—The study was conducted on Browns Island, a natural brackish tule-dominated high-stand marsh in the tidal reaches of San Francisco estuary (SFE, Fig. 1).

Island soils are derived of humified plant remains and thus have the high organic content and low bulk densities typical of historic marshes in the region. Tides in SFE near Browns Island are mixed semidiurnal, with a maximum spring tidal range of 1.8 m and a minimum neap tidal range of 0.20 m. The regional water surface elevation varies seasonally, with higher stages in the winter months during high river flows. The island contains a well-defined main channel on the northern side, and a primary side channel on the southern side that drain the majority of the island, both of which were instrumented at locations suitable for flux calculations (Fig. 1). The marsh plain is approximately 1 m above mean low low water, and thus the island is inundated during high spring tides.

Sample collection—For each deployment period, discrete samples integrating the cross section were collected by boat hourly over a 24-h period during the predicted maximum tidal range. To ensure samples were representative of the full channel cross section at each tidal stage, samples were collected at five equal discharge increments (EDI) across the channel and vertically integrated with the use of an isokinetic D-77 bottle sampler fitted with a 0.25-inch (0.64-cm) nozzle (Ganju et al. 2005; Downing et al. 2009).

For mercury sampling, a slightly modified version of U.S. Environmental Protection Agency (EPA) Method 1669 (EPA 1996) was used. Samples were collected with clean techniques using an acid-washed, 3-liter Teflon bottles and nozzle. One aliquot each was collected for unfiltered MeHg, and another was filtered using specialized Hg-clean Teflon filtration system (0.45 μm, No. 12178, Pall; Puckett and Buuren 2000). Filtration of MeHg samples was typically conducted immediately on-board, but also on occasion in the laboratory within 24 h when on-board filtering was not possible. Samples were preserved with trace metal–grade HCl immediately after aliquot processing and stored chilled ($< 4^{\circ}$C) until analysis. Field blank values of deionized water were below the method detection limit. Dissolved organic carbon (DOC) samples were decanted immediately, gravity filtered through a 0.3-μm glass fiber filter (Advantec MFS) into amber glass vials, transported on ice, stored chilled ($< 4^{\circ}$C), and analyzed within 24 h.

Laboratory procedures—MeHg concentrations were determined by EPA (1998) method 1630, as described by Choe et al. (2003). In brief, 50–80 mL of acidified sample with ammonium pyrrolidine dithiocarbamate added as a matrix modifier was distilled, buffered, reacted with 1% sodium tetraethylborate, and volatilized for collection on a Carbotrap™ column (Supelco). Products were then separated by gas chromatography for subsequent determination using cold vapor atomic fluorescence spectrometry. The method detection limit (MDL) for MeHg determinations was 0.02 ng L^{-1}. Relative percent deviation between duplicate analyses averaged 14%. Results from the filter-passing fraction of MeHg are defined here as ''dissolved'' (DMeHg) for clarity, with the express understanding that colloidal material can comprise a significant contribution. The difference between the unfiltered whole water (UMeHg) and DMeHg is defined as ''particle-associated'' or ''particulate'' (PMeHg).

Bulk DOM (reported as DOC) was measured by high-temperature catalytic oxidation with a Shimadzu TOC-5000A total organic carbon analyzer (Bird et al. 2003). Absorbance at 254 nm (A_{254}) was determined using an absorbance spectrophotometer with a 1-cm path length (Model UV-Vis Lambda 3B, Perkin-Elmer). Samples with A_{254} values greater than 1.2 were diluted and reanalyzed.

In situ deployments—A moored instrumentation system (Downing et al. 2009) was deployed at two slough locations (Fig. 1) during three seasons: Spring (13 April 2005–09 May 2005), Fall (05 October 2005–26 October 2005), and Winter (11 January 2006–01 February 2006). Instrumentation was moored, with sample intakes approximately 1 m above the channel bottom.

The fluorescent fraction of DOM (FDOM) was measured using a WETStar colored dissolved organic matter (CDOM) fluorometer, with excitation centered at 370 nm and emission centered at 460 nm (WETLabs). The spectral absorption (a_g) was measured on the filtered flowpath (0.2 μm; Memtrex, Osmonics) using the absorption (a) side of a WETLabs model *ac*-9 spectrophotometer. Spectral properties of whole water were measured on the unfiltered flowpath using the attenuation (c) side of the *ac*-9 (c_{pg}). Optical properties of the particulate fraction (c_p) were obtained by subtracting the absorption measurements (a_g) of the dissolved flowpath from the measurements obtained from the attenuation cell ($c_p = c_{pg} - a_g$), assuming scattering of dissolved matter is negligible.

Apart from the optical instrument package, conductivity, salinity, pressure (Sea-Bird model SB37-SI, Sea-Bird Electronics), water temperature, pH, and turbidity as backscatter at 860 nm (Hydrolab) were measured. Data were collected for 2 min at 30-min intervals. Refer to Downing et al. (2009) for details on instrumentation and deployment protocols.

Index water velocities were measured in situ using an upward-looking acoustic Doppler velocity meter (ADVM; Sontek Argonaut XR, Sontek) deployed on the main channel bed as described by Ganju et al. (2005). The ADVM was placed in close proximity to the optical package and collected depth-averaged velocity and water depth above the unit every 15 min for 6 min. Surveys were conducted over maximum spring tides during each deployment using a downward-looking acoustic Doppler profiler to relate the cross-sectional area to depth and average velocity (u) to the index velocity at every tidal phase.

Meteorological data used in this study were from the Twitchell Island, Concord, and Hastings Tract sites of the California Irrigation Management Information System (CIMIS) network (www.cimis.water.ca.gov).

Data processing—Data were processed as described in Downing et al. (2009). Data from each in situ sensor was binned to a 30-min interval by averaging the last 10 s of each 2-min sampling period. Baseline offsets were removed using a calibration correction or a simple linear correction between service intervals where necessary. Following

baseline corrections, service breaks were filled using cubic spline interpolation to generate continuous, 30-min time series.

Spectral slope (S), known to be a relative indicator of composition, was calculated from *ac*-9 data with a nonlinear least squares curve-fitting technique. The absorption (a_g) data from 412 to 650 nm were used to determine S_{ag}, with higher values related to lower molecular weight or fresher organic materials (Twardowski et al. 2004). Similarly, the particulate attenuation (c_p) spectrum from 412 to 650 nm was used to determine the slope of c_p (S_{cp}) with a nonlinear least squares (power) fit, which is related to the shape of the particle size distribution, with lower values related to a higher median bulk particle size (Boss et al. 2004).

Time series modeling—Partial least squares regression models were developed (Unscrambler, Camo Software) to relate the in situ index measurements made in the center of the channel to the measured filtered and unfiltered MeHg values from the integrated EDI samples collected across the channel section. The models related UMeHg and DMeHg to in situ fluorescence, absorption, and attenuation measurements across all deployments. Individual predictive variables were normalized by their standard deviation. Models were fully cross-validated with a stepwise sample exclusion routine to ensure outlier samples did not dominate the analysis. The fit of the model was evaluated as the correlation between the observed MeHg concentrations and those predicted by the model. Model parameters were chosen solely to provide relationships to physical and geochemical processes rather than to improve model fit.

The DMeHg model used FDOM and absorbance wavelengths (a_g) of 412, 440, 512, and 555 nm from the filtered flow path. All wavelengths used in the model had considerable predictive power for DMeHg, similar to that of 412 nm (Table 1). For the UMeHg model, because UMeHg contains both particulate and dissolved MeHg, the spectral slope of the particulate material (S_{cp}) and total attenuation (c_{ag}) used wavelengths 412, 440, 488, 510, 532, 555, 650, and 676 nm from the unfiltered path to account for the contribution of particle composition and concentration (Boss et al. 2004). To account for the DMeHg contribution, we used the same parameters as used for the DMeHg model, along with the spectral slope of the dissolved fraction (S_{ag}) as an indicator of water provenance. With these parameters, the model explained a total of 83% of the variability in UMeHg concentrations over all three sampling periods in our study (Fig. 2).

Efforts to model the PMeHg time series directly were frustrated by insufficient variability in properties during the period of discrete sampling and because of the high error in the analytical determination by difference. To develop the PMeHg time series, we subtracted the DMeHg concentration time series from the UMeHg time series—the same method used to calculate PMeHg in the discrete samples. There are significant issues in modeling PMeHg with this approach: the model produces negative concentration values during some periods of the study. Although the negative concentrations were censored for the purpose of calculating flux, their occurrence indicates the model parameters developed from the discrete sampling periods did not adequately capture the variability observed over the full deployment period. Comparison of the modeled PMeHg concentrations to the available measured values indicated only 23% of the variability was explained by the model (Fig. 2). Accordingly, the modeled PMeHg concentrations should be regarded as heuristic rather than quantitative; it is presented to facilitate understanding of processes and constrain magnitude and variability.

Flux calculations—Water flux from each channel was calculated for each 15-min interval according to Downing et al. (2009) and Ganju et al. (2005) as the product of the derived cross-sectionally averaged velocity and the tidal phase–dependent cross-sectional area provided by the surveys. Measured water fluxes did not balance over the deployment period, meaning some of the water passing our measurement location during flood was not measured during ebb. The imbalance was greatest during spring tides, suggesting that water from these high tides likely escapes across the marsh plain or ebbs principally through yet smaller channels distributed around the island, but concentrated on the south side (Fig. 1). Ganju et al. (2005) reported a net water imbalance of 22% on the island using two similar deployment locations and suggested that a combination of seepage, overland flow, and minor channels on the south side of the island accounted for the missing water.

Constituent fluxes were calculated as the product of the water flux and the constituent concentration. To calculate constituent fluxes, we forced closure in the water budget over the calculation period, taking into account the effects of precipitation, evapotranspiration, and any change in storage (Ganju et al. 2005; Downing et al. 2009). For the purposes of our calculations, the unaccounted-for water necessary to force closure in the water budget was assigned the concentration properties of side-channel water. We judged that the smaller, shallower, lower volume side channel best represented the unaccounted-for water ebbing through the small channels.

Because a survey indicated Browns Island is virtually flat (data not shown), the yield (flux per unit area) was crudely estimated by defining the contributing area as a function of simple water exchange: the volume of water exchanged divided by the change in water height. The area of yield was calculated as the volume of the flooding waters during the highest tide occurring in the deployment period divided by the change in water height over that tide, adjusted to account for the water retained in the soils and the volume of the soil itself. We estimated the moisture content to be an average of 50% during drained conditions (Boelter 1964; Weiss et al. 1998) and the soil porosity to be 0.9 (Fleck et al. 2007), resulting in a contributing area 1.8 times the area defined by the simple water exchange. This method provides a rough estimate of the tidal drainage area, representing approximately 30% of the total island area in Winter, 20% in Fall, and 15% in Spring, consistent with the locations of the sampling stations, which would only

Table 1. Correlation coefficients for relation of dissolved, unfiltered, and particulate methylmercury to selected parameter for Browns Island study. Entries with absolute values greater than 0.41 are significant at the 99% level. Separate relationships are shown for *all samples* in the study, for the subset of all samples collected on the *ebb*, and the subset of all samples collected on the *flood*. Ebb is defined as any period with a negative, off-island discharge, and flood is defined as any period with a positive, on-island discharge. (A) Grouped by common measured chemical and physical parameters. (B) Grouped by the three monomethylmercury phases. (C) Grouped by selected spectrophotometric measurements made in situ. (D) Grouped by selected dissolved and particulate quality parameters derived from measured spectral properties. Note that temperature and conductivity relationships are driven by seasonal trends. *See* text for discussion.

	All samples			Ebb samples			Flood samples		
	DMeHg	UMeHg	PMeHg	DMeHg	UMeHg	PMeHg	DMeHg	UMeHg	PMeHg
A. Physical and chemical parameters									
DOC	0.94	0.8	−0.08	0.94	0.73	−0.1	0.95	0.89	−0.18
POM	−0.44	−0.03	0.69	−0.48	0.12	0.75	−0.4	−0.42	0.47
SSC	−0.09	0.28	0.63	−0.18	0.34	0.72	0.04	0.16	0.6
TURB	−0.06	0.18	0.57	−0.1	0.28	0.75	−0.01	0.03	0.41
COND	−0.75	−0.76	−0.08	−0.72	−0.74	−0.13	−0.78	−0.82	−0.05
T	−0.8	−0.69	0.1	−0.76	−0.56	0.17	−0.83	−0.88	−0.12
DO	−0.39	−0.13	0.21	−0.48	−0.05	0.34	−0.31	−0.1	0.37
Depth	0.21	0.25	0.33	0.29	0.49	0.5	0.13	0.05	0.17
u	0.05	−0.3	−0.54	0.18	−0.26	−0.7	−0.07	−0.05	0.34
Q	0.03	−0.31	−0.53	0.16	−0.28	−0.71	−0.11	−0.08	0.39
B. Internal									
DMeHg	–	0.69	−0.25	–	0.54	−0.31	–	0.93	−0.13
UMeHg	0.69	–	0.55	0.54	–	0.62	0.93	–	0.26
PMeHg	−0.25	0.55	–	−0.31	0.62	–	−0.13	0.26	–
C. In situ spectrophotometric parameters									
FDOM	0.95	0.76	−0.16	0.95	0.66	−0.22	0.95	0.95	0.01
*a*412	0.94	0.75	−0.17	0.95	0.62	−0.28	0.93	0.95	0.09
*a*440	0.9	0.76	−0.11	0.91	0.65	−0.21	0.88	0.94	0.19
*a*488	0.77	0.7	−0.06	0.78	0.57	−0.19	0.77	0.9	0.34
c_{p650}	0.32	0.36	0.26	0.28	0.42	0.39	0.39	0.36	0.24
D. Derived quality parameters									
BB : B	−0.47	−0.18	0.45	−0.44	0	0.66	−0.53	−0.47	0.18
S_{Cp}	0.7	0.43	−0.43	0.76	0.27	−0.6	0.68	0.61	−0.47
S_{ag}	−0.17	0.12	0.54	−0.09	0.47	0.83	−0.26	−0.29	0.01
RFE	0.96	0.73	−0.25	0.97	0.49	−0.35	0.96	0.93	−0.03

DMeHg, filter-passing fraction of methyl mercury; UMeHg, methyl mercury in whole-water samples; PMeHg, particulate methyl mercury calculated as the difference between unfiltered and dissolved; DOC, dissolved organic carbon; POM, particulate organic matter as carbon; SSC, suspended sediment concentration; TURB, turbidity as derived from optical backscatter; *T*, temperature; *u*, velocity; *Q*, discharge with flood defined as positive; FDOM, fluorescence at excitation of 370 nm and emission at 450 nm; DO, dissolved oxygen; *a*412–*a*488, the absorption of filtered measurements at the nominal wavelength indicated; c_{p650}, the particle attenuation at 650 nm; BB : B, ratio of the turbidity and particulate beam attenuation at 650 nm—an indicator of the index of refraction of particles (Boss et al. 2009); S_{Cp}, slope of the attenuation spectrum due to particles; S_{ag}, slope of the absorbance spectrum of filtered measurements, which is a concentration-independent parameter related to organic matter composition; RFE, relative fluorescence efficiency defined as the FDOM divided by the absorbance at 370 nm; estimated using S_{ag}.

capture a fraction of total island drainage. It should be noted that this calculation uses the area determined at the maximum tide height during the deployment, and the lower tidal exchange during lower tides would result in a smaller derived contributing area and, thus, a higher calculated yield. However, this may be offset by an unknown amount because of lower head differences during lower tides (Weiss et al. 1998).

Validation, error analysis, and uncertainty—For the concentration models, the root mean square error of prediction (RMSEP) for the DMeHg model was 0.012 ng L^{-1} and for the UMeHg model was 0.024 ng L^{-1}. Model validation was within 0.04% of the calibration values. Additional empirical validation was obtained by omitting a series of measurements from the model development and combining prediction residuals to compute the RMSEP.

For the flux, the largest single contributing error involved in the seasonal MeHg flux calculations was associated with estimations of the channel-averaged MeHg concentration consisting of three primary components: (1) errors inherent in the measurement method in representing actual channel-averaged conditions, (2) errors in the MeHg lab measurement, and (3) errors associated with the partial least squares regression models.

Errors inherent in the equal discharge increment (EDI) method have been reported in the range of 8–11%. Because of lateral and vertical variations, the EDI method cannot precisely measure the channel-averaged concentrations (Ganju et al. 2005). The laboratory error in DMeHg

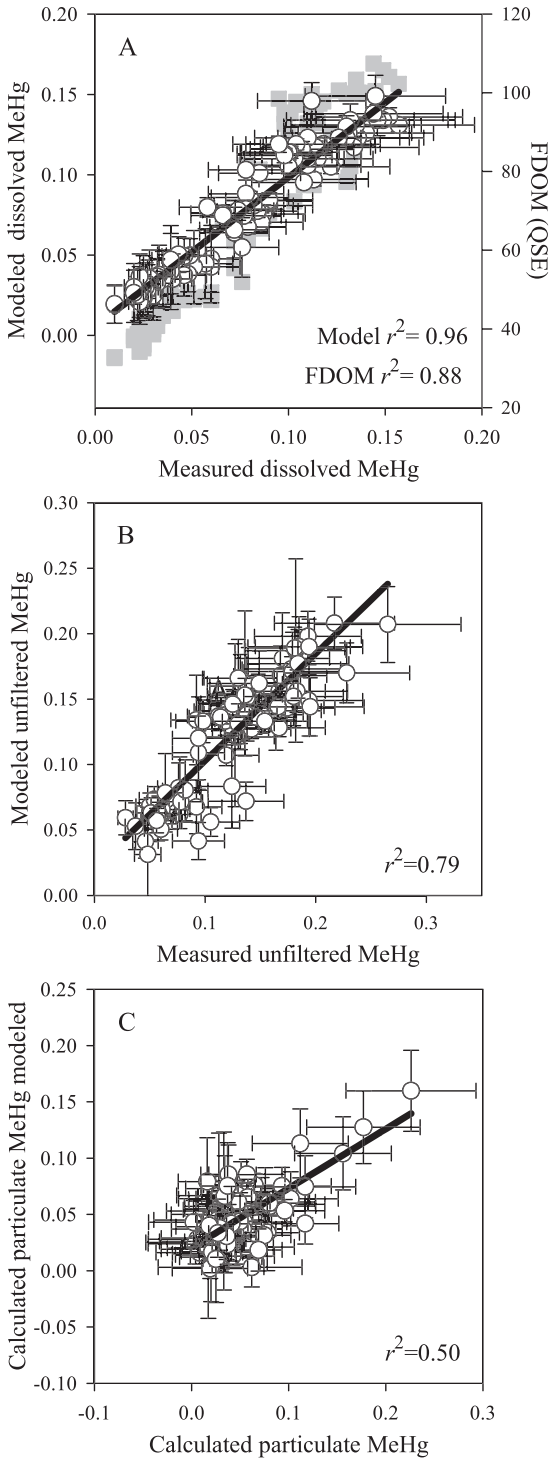

Fig. 2. Comparison of measured and modeled values for (A) dissolved, (B) total, and (C) particulate MeHg (μg L^{-1}). (A, B) Horizontal error bars show error in measured values. (C) Horizontal error bars show compounded error accrued calculating the particulate values from the total and dissolved measurements. (A, B) Vertical error bars show error of prediction for model (*see* Methods section for discussion). Vertical error bars in panel C show compounded error accrued calculating the particulate values from the total and dissolved models. Note that analytical error and model error are of similar in magnitude. (A) Gray squares show fluorescent dissolved organic matter (FDOM) measurements for comparison.

measurements is 14% of the measured value for samples with DMeHg greater than 1 ng L^{-1}. The uncertainty in MeHg flux was calculated analogously to that presented in Ganju et al. (2005) and was less than 25%, on the basis of 6% uncertainty in modeled MeHg values, and assuming the uncertainties in water velocity and modeled MeHg to be uncorrelated. This is compared with a calculated uncertainty in the sediment flux of 27%, as presented previously in Ganju et al. (2005).

Results

Dissolved MeHg—For all sampling periods, concentrations of dissolved MeHg (i.e., filter-passing; DMeHg) increased as the tide ebbed to a peak near low water, and then steadily declined during flood (Figs. 3, 4). The absolute concentrations as well as the concentration range were significantly different between seasons. For the Winter deployment, values ranged from 0.06 to 0.16 ng L^{-1} at high and low tide, respectively. For Spring, the concentrations were lower, ranging from 0.04 ng L^{-1} to 0.13 ng L^{-1} at high and low tide, respectively. In Fall, the observed concentrations were much lower, ranging from below the MDL at high tide to 0.05 ng L^{-1} at low tide. It should be noted that the peaks in DMeHg concentration correspond to the lowest stage of the tide, whereas the minima do not correspond to the highest stage (Fig. 3).

For the ancillary parameters measured on the discrete samples, DMeHg varied most closely with DOC (r = 0.94; Table 1), as well as temperature and conductivity. Concentrations of DMeHg were poorly related to water depth, velocity, and discharge, even when segregated into ebb and flood samples (Table 1). Several of the parameters measured in situ were also strong predictors of DMeHg. For example, FDOM—a broad-spectrum measurement of fluorescence related to concentration of dissolved humic material—was highly related, as has been previously reported (Hill et al. 2009) for discrete samples. Other DOM concentration–related parameters, such as absorption at λ_{412} and λ_{440}, had similarly high correlations ($r \geq$ 0.90; Table 1). Significantly, the concentration-independent DOM quality parameters derived from in situ data, S_{ag} and relative fluorescence efficiency (RFE), were similarly highly related (Table 1). The RFE normalized to DOC (r = 0.9) in particular was highly related on both flood and ebb tides.

Time series of dissolved MeHg—The final dissolved concentration model explained 96% of the variability, similar to FDOM alone, which explained 88% (Fig. 2). Using multiple parameters reduces the effects of spurious events and offers the advantage of relating concentrations to a variety of biogeochemical processes. Variation in the modeled DMeHg concentration time series generally agreed with the discrete sample measurements and reflected the differences resulting from the semidiurnal tides and the longer period spring–neap fluctuations (Figs. 3, 6). As for the discrete data, significant differences exist between seasons in the time series data. Side channel peaks in DMeHg concentration were generally much lower than the main channel, but baseline values were similar in magni-

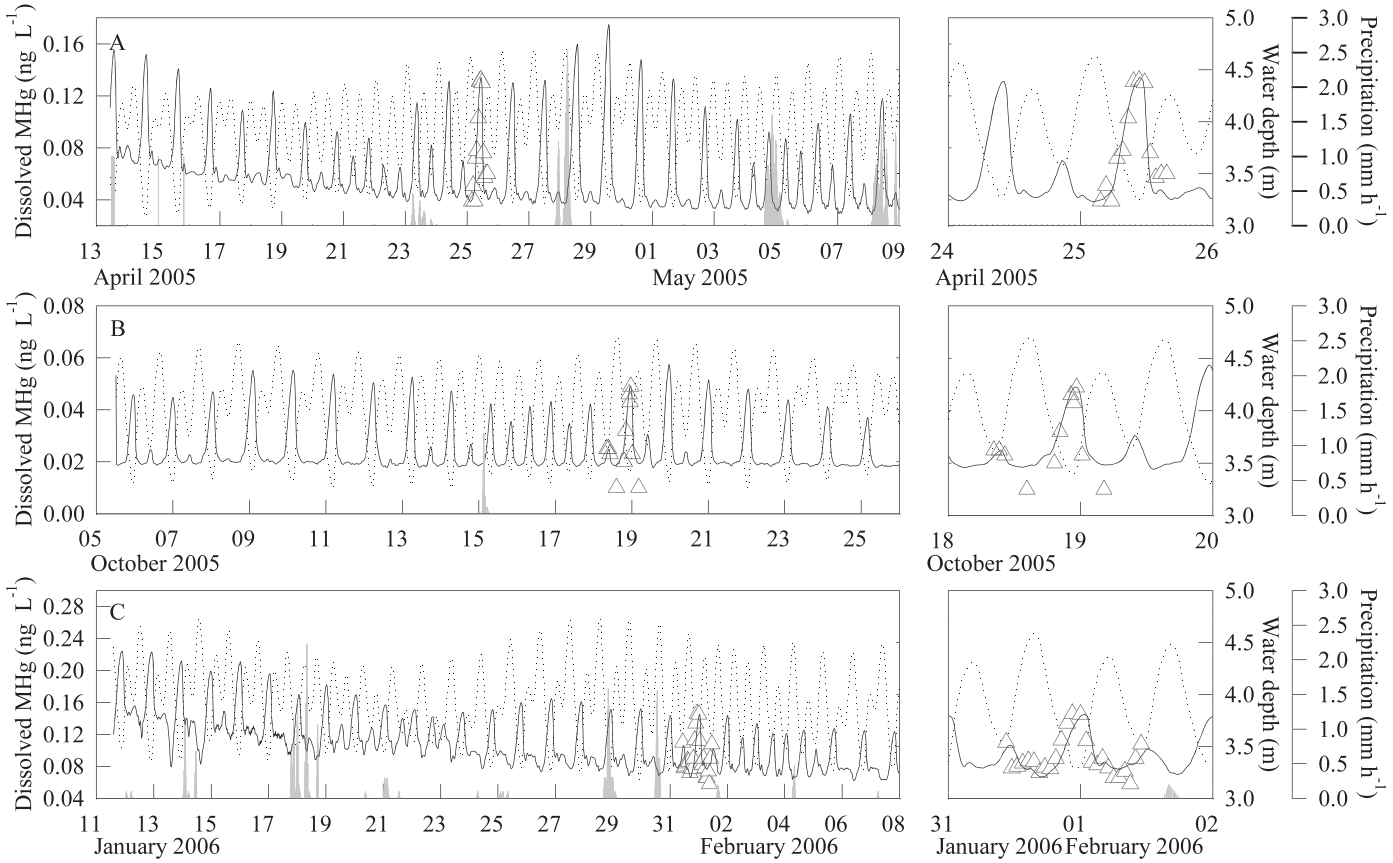

Fig. 3. Time series of dissolved methylmercury in main channel site on Browns Island for (A) Spring, (B) Fall, and (C) Winter deployments. Right-hand panel is expanded view over sampling period. Discrete sample measurements shown as symbols; modeled dissolved MeHg concentration time series shown as solid line; water depth shown as dashed line; precipitation shown as gray bars.

tude (Fig. 4), as would be expected because the source waters were the same. These observations provide confidence in the model used to develop the time series from in situ measurements.

Flux of dissolved MeHg—Flux calculations indicate Browns Island was a net source of MeHg to the greater estuary throughout the year, but the flux varied with season, local conditions, and events (Table 2). The cumulative rise in flux associated with tidal exchange was clearly the dominant process (Fig. 5). On a net basis, fluxes were off-island for all seasons, with approximate DMeHg fluxes calculated for the Winter of 5 mg, for the Spring of 24 mg, and for the Fall of 14 mg over a full lunar tidal cycle (Table 2). Note that the fluxes varied considerably over the sampling period, with occasional periods of on-island flux.

Precipitation also affected single-tide flux, as seen in three enhanced total off-island fluxes of DMeHg in Spring (5, 9, and 18 mg; sum of baseline and event flux; Table 2). Two of the enhanced DMeHg fluxes occurred within the springing tide period, accounting for half the DMeHg flux during that period. Although there were only three minor rainfall events, they accounted for a considerable amount of the total flux over the deployment period (Table 2). It should be noted, however, that the effects in Spring are discernable because the precipitation events are discrete. In Winter, the precipitation events are too numerous to assess the effects of individual events, but total calculated fluxes are lower. It is highly unlikely the increased flux was due to MeHg in rain because concentrations in rain are low (Selin 2009). The DMeHg flux appears unaffected by wind events with an off-island flux of about 1 mg per cycle throughout the record in Spring and Fall, except when a strong north wind countered the tidal ebb of water in Winter and consequently caused an on-island flux of DMeHg during this period (Fig. 3).

Unfiltered and particulate MeHg—The highest observed range of UMeHg measured in discrete samples was in Spring (0.09–0.26 ng L^{-1}; Figs. 6, 7), with smaller ranges in Fall (0.03–0.14 ng L^{-1}) and Winter (0.11–0.22 ng L^{-1}). The observed range in PMeHg for the discrete samples in the Winter and Fall were similar, from 0.02 to 0.12 ng L^{-1}, but the range of observed concentration was higher in the Spring deployment, from below the MDL to 0.23 ng L^{-1} (Figs. 8, 9). Both the main and side channels were similar in UMeHg and PMeHg concentrations despite the differences in residence times and current velocities. The PMeHg fraction of the total was clearly higher than the DMeHg in 10% of the samples, and concentrations were relatively similar in 40% of the samples, in contrast to what has been observed elsewhere, wherein dissolved concentrations were

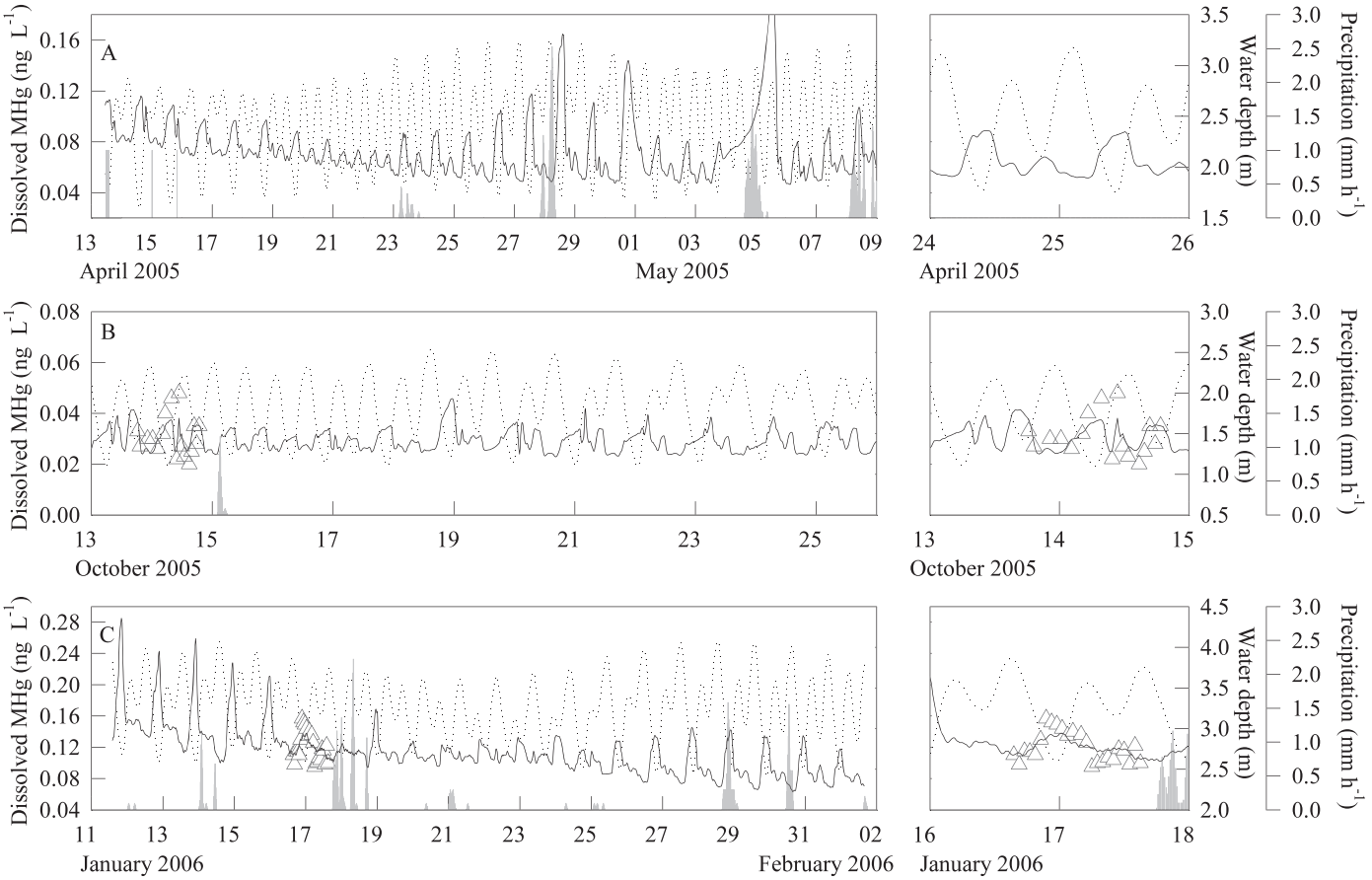

Fig. 4. Time series of dissolved methylmercury in side channel site on Browns Island for (A) Spring, (B) Fall, and (C) Winter deployments. Right-hand panel is expanded view over sampling period. Discrete sample measurements shown as symbols; modeled dissolved MeHg concentration time series shown as solid line; water depth shown as dashed line; precipitation shown as gray bars. Discrete samples were not collected during Winter in the side channel during the monitoring period.

generally higher (Hill et al. 2009). Winter was the only season in which DMeHg generally comprised the majority fraction of UMeHg (> 90%). It is notable that the MeHg content of the particulates was enhanced in ebbing waters (5 ng g^{-1}) compared with flooding waters (1 ng g^{-1}) and appeared to be most closely related to the organic content of the particles—but the ratio of MeHg to OC differed between seasons (Figs. 6, 7; Table 1).

For the parameters measured on discrete samples, PMeHg covaried most strongly with particulate organic matter (POM; Table 1; $r = 0.7$), and suspended sediment (SSC; $r = 0.6$). Discharge (Q) and velocity (u) were strongly related to PMeHg on ebb ($r = 0.5$–0.7), but not on flood. The backscatter ratio (BB : B) and the slope of the attenuation spectrum (S_{Cp}), both indicators of particle quality (Boss et al. 2001, 2004), were also strongly related on ebb, but not on flood, indicating particles of different quality were present in ebbing waters ($r > 0.6$). However, the relationship with c_{p650}, a proxy for particle concentration, was similar on ebb and flood, suggesting this was not due to a change in particle concentration (Table 1).

Time series of unfiltered and particulate MeHg—The modeled UMeHg concentrations were clearly tidally influenced, but not to the same degree as DMeHg (Figs. 3, 6). The modeled PMeHg concentrations exhibited greater variability than the DMeHg time series, but the variability was not primarily coupled to tides (Figs. 8, 9) and was different between seasons. Tidally coupled modeled concentrations of PMeHg varied from a baseline of 0.08 ng L^{-1}, with peaks above 0.16 ng L^{-1}. In Fall, baseline concentrations were near 0.04 ng L^{-1}, with smaller peaks of up to 0.10 ng L^{-1}. Winter exhibited similarly low baseline concentrations—from below detection levels to 0.04 ng L^{-1}; intertidal variability ranged to near 0.8 ng L^{-1}.

Flux of unfiltered and particulate MeHg—The net flux of UMeHg and PMeHg was off-island in all seasons, but varied during the spring–neap tidal cycle (Fig. 5). For example, neaping tides led to net on-island fluxes of PMeHg in Spring (4 mg $tide^{-1}$), whereas springing tides led to off-island fluxes of PMeHg (3–7 mg $tide^{-1}$; Table 2, Fig. 5).

In Fall and Winter, large event-related on-island fluxes were associated with high winds and high suspended sediment concentrations. Although the material resuspended by wind waves and swept onto the island by the rising tide was not sampled and included in the MeHg

Table 2. Total, tidal, and event-related MeHg fluxes for Browns Island (mg). Totals are for entire spring neap period. Negative values are off-island. Event values were estimated as the flux minus the baseline flux for the period of measurement.

	MeHg flux (mg)					
Season and phase	Total	Springing tide avg	Neaping tide avg	Rain event	Wind event	Notes
Spring						
DMeHg	−24	0	−3	−2 to −15	No effect	
PMeHg	−34	−4	−7	No effect	No effect	
UMeHg	−58	−4	−10	−2 to −15	No effect	
Fall						
DMeHg	−14	−1	−1	na	No effect	
PMeHg	−25	−4	0±2	na	+24 to −11	The wind event caused an on-island flux followed by an off-island flux
UMeHg	−39	−5	−1	na	+24 to −11	
Winter						
DMeHg	−5	−5	−4 to +7	Unknown	+14 to +3	Too many events during spring–neap cycle to estimate average DMeHg
PMeHg	−72	−7	−7	Unknown	37	Effects of rainfall difficult to decouple from record
UMeHg	−77	−12	−11 to 0	Unknown	+51 to +40	

avg, average; na, not applicable; other abbreviations as in Table 1.

concentration model, the use of ambient MeHg content and higher observed suspended sediment concentrations (*see* Methods) yielded a modeled on-island flux of 20 mg PMeHg in Fall and 30 mg in Winter (Fig. 5). In Fall, following the elevated on-island flux event, an enhanced off-island PMeHg intertidal flux (8 and 15 mg) was observed during springing tides (Table 2, Fig. 4), suggesting some of the storm-deposited material was returned to surrounding channel waters.

Discussion

The combination of the modeled MeHg time series and discrete measurements yield new insights into wetland exchange processes. The time series data indicate that the particulate and dissolved pools were largely independent in this system, with the tidal maxima in the DMeHg time series near low slack water and minima near the highest stage for any given tide. In contrast, the highest PMeHg concentrations were observed on flood tides associated with storm events and depended on the direction of the wind. Nevertheless, PMeHg concentrations were tidally coupled, with elevated concentrations of PMeHg occurring systematically during ebb. The time series data also permit examination across temporal scales. For example, the importance of spring–neap cycles in driving concentration and flux is readily seen (Figs. 3–9).

Dissolved MeHg—Baseline DMeHg concentrations were significantly different between seasons, with Winter exhibiting the highest ($\sim$ 0.09 ng L^{-1}; Fig. 3) and Fall the lowest ($\sim$ 0.02 ng L^{-1}). These seasonal changes in background DMeHg were continuous, as was apparent in the relatively short timescale of the in situ deployments; both Winter and Spring time series exhibited a systematic change in background concentrations over the deployment period (Figs. 3, 4). The change corresponded to a general regional decline in dissolved organic carbon (DOC) concentrations in Sacramento and San Joaquin Rivers (California Data Exchange Center [CDEC] 2010), consistent with a flushing of DOC impounded in the Central Valley hydrologic system. The seasonal differences in baseline concentrations account for strong relationships of DMeHg to temperature and conductivity (Table 1).

Variation in DMeHg concentration during tidal exchange has been observed by others (Mitchell and Gilmour 2008), and our data show that peaks in DMeHg concentration increased progressively during ebb as water drained from the wetland surface and soils into the channel. Concentrations crested at low water and declined during flood as river water enters the wetland channel until it reached the regional baseline concentration value, representative of unmixed river water. The peaks are asymmetric, however, with generally a more rapid rate of change during falling concentrations than during rising concentrations due to the mixing of wetland water into the regional surface water system during each tide, but the effect varies by season (Fig. 3).

The spring–neap tidal cycles also strongly affected DMeHg concentrations, with the excursion from baseline concentration values largest during spring tides (Fig. 3). This effect is not symmetrical around the peak in tidal range, however, with the modeled DMeHg concentrations lagging the largest spring tides by several tidal cycles for all seasons (Fig. 3). This observation does not support our conceptual model; simple hydrologic reattachment of distal wetland zones during spring tides did not immediately release pools of MeHg formed during the period of

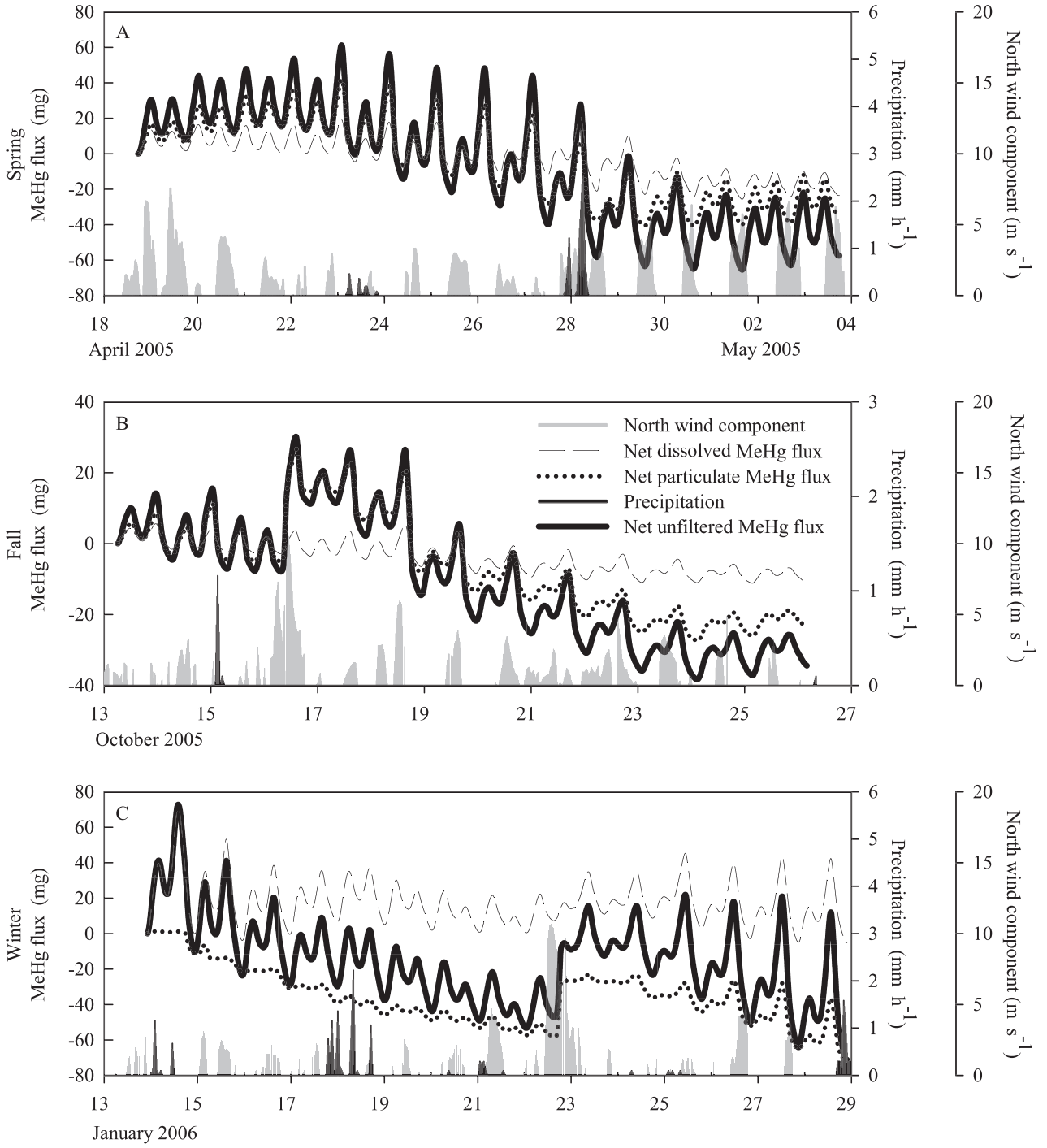

Fig. 5. Cumulative net fluxes of dissolved (dashed line), unfiltered (solid line), and particulate (dotted line) methylmercury over time for a full spring–neap cycle on Browns Island for (A) Spring, (B) Fall, and (C) Winter deployments. Black bars show precipitation. Gray bars show northern component of wind. Off-island flux is defined as negative.

detachment. It is only after maximum tide heights recede that peak concentrations return to values symmetric to springing tide heights (Fig. 3). This observation suggests that MeHg production might be limited or MeHg losses enhanced in detached areas away from tidal channels and that tidal inundation is needed to restore conditions conducive for release into tidal channels. However, the lag is similar in magnitude regardless of the riverine sulfate concentration, which varies from 8 to 35 μg L^{-1} during high flows in Winter, from 10 to 40 μg L^{-1} in Spring, and from 100 to 500 μg L^{-1} during low flows in Fall (CDEC 2010). This indicates the supply of sulfate or build up of sulfide is not likely to be limiting to MeHg production. It seems likely, therefore, that the lag evinces an induction

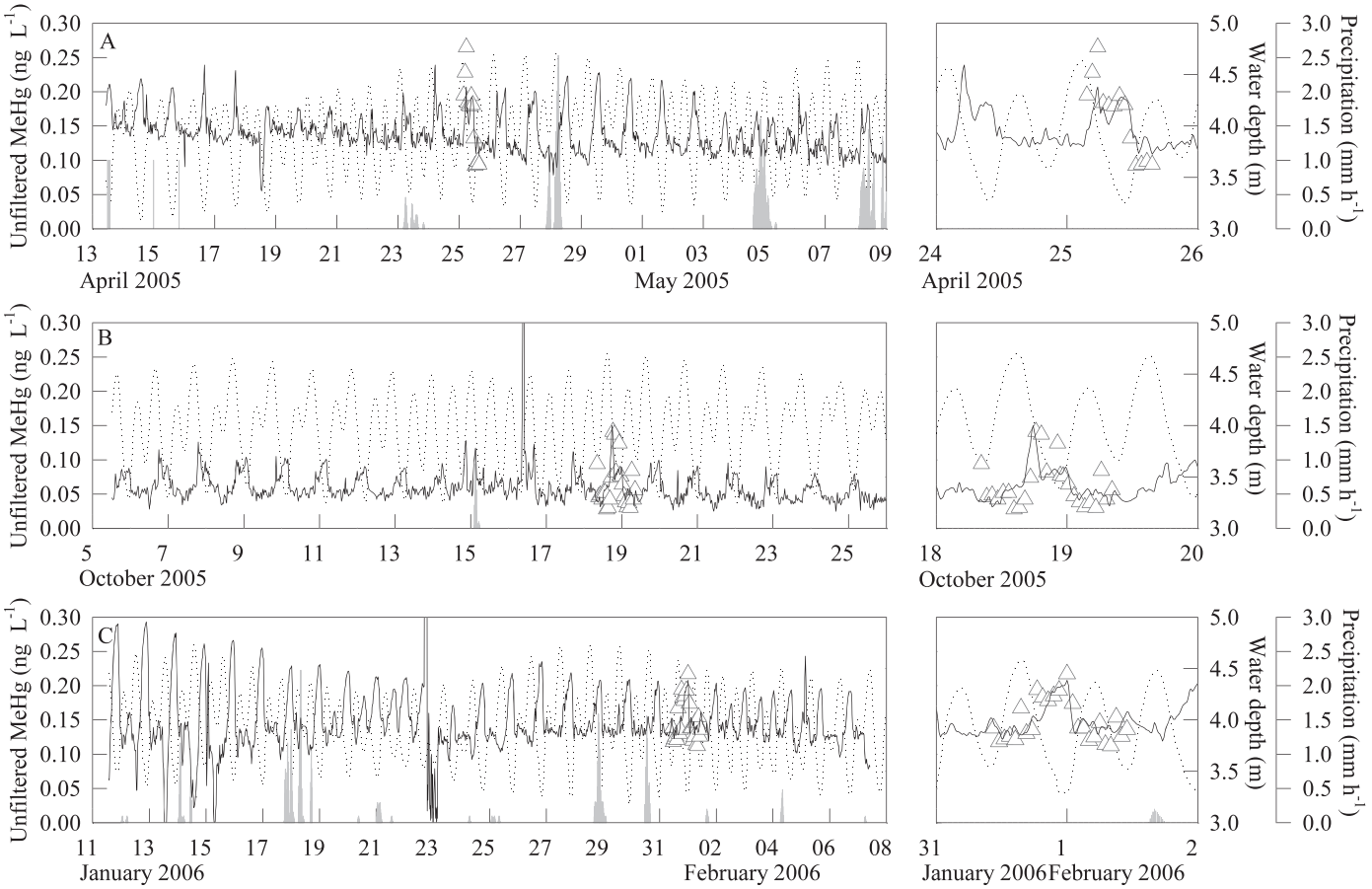

Fig. 6. Time series of unfiltered methylmercury in main channel site on Browns Island for (A) Spring, (B) Fall, and (C) Winter deployments. Right-hand panel is expanded view over sampling period. Discrete sample measurements shown as symbols; modeled unfiltered MeHg concentration time series shown as solid line; water depth shown as dashed line; precipitation shown as gray bars.

period necessary to restore redox conditions amenable to sulfate reduction after the week-long exposure of the marsh plain during low tide heights. This is supported by the increased DMeHg concentrations seen after some rain events and some instances when stage was affected by wind or barometric pressure. Additionally, the absence of change in DMeHg concentration once water levels exceed the height of the marsh plain, (both inter- and intratidally) shows that mere inundation of the marsh plain does not increase DMeHg concentrations, suggesting that DMeHg production is not solely due to methylation of newly deposited sedimentary or atmospheric mercury or a consequence of exposure to labile detrital material on the marsh plain.

Although significant loss of DMeHg can occur in aquatic systems (Marvin-Dipasquale et al. 2000), seasonal and time series data indicate these that losses due to photodemethylation (Sellers et al. 1996), partitioning to sediments (Bengtsson and Picado 2008), or microbial oxidation (Whalin et al. 2007) were not dominant at Browns Island. The effects of photodemethylation would be evident from a comparison of the DMeHg : DOC ratios (values not shown) between the confined main channel and the large open-water area associated with the side channel. Our data show that the peaks in the ratio were similar between the two sites, indicating photodemethylation was not appreciable over the residence times of the side channel or that DOC loss to photolysis was proportionally the same as any DMeHg loss. Sediment partitioning would affect the same ratios when tide heights overbank and flood the marsh plain, permitting interaction with storm sediment deposits, but no effect was observed. The similar relationship between DOC and DMeHg across seasons suggests that the range of temperature, sulfate supply, and oxygen solubility—and thus biotic attenuation—was also not important.

Unfiltered and particulate MeHg—The largest features in the modeled UMeHg and PMeHg time series are episodic in nature, occurring once each in the main channel Fall time series and seen in both the main and side channels in Winter (Figs. 6–9). These episodes were associated with short-duration wind events, wherein shallow water waves resuspend bed sediment for a short period of time (Schoellhamer 2002) but elevate the PMeHg concentrations by a factor of 20 or more above baseline, although the model is not calibrated to event concentration data. The higher modeled PMeHg values during events are driven by the high observed water column suspended sediment concentrations, rather than a greater amount of MeHg

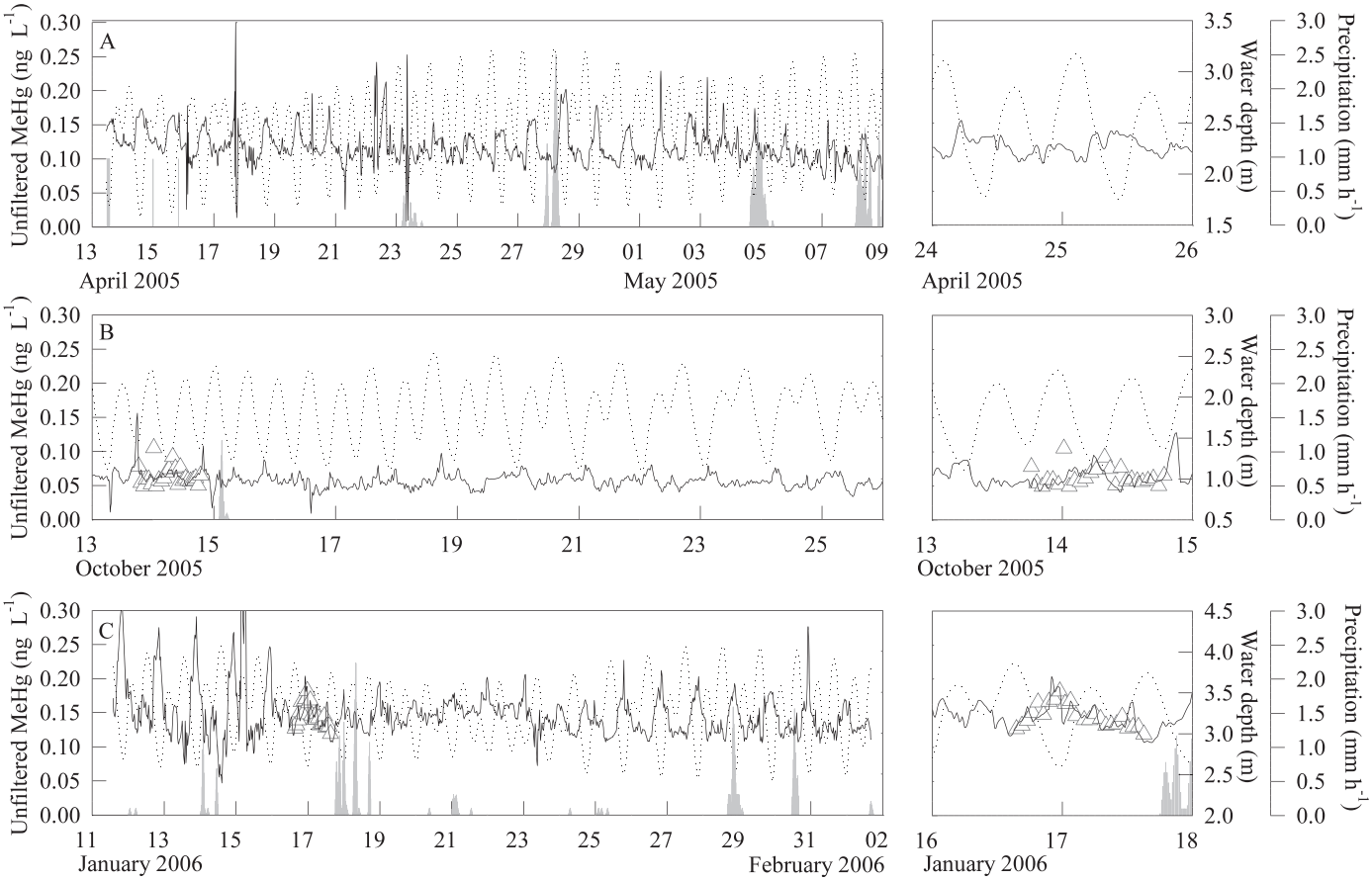

Fig. 7. Time series of unfiltered methylmercury in side channel site on Browns Island for (A) Spring, (B) Fall, and (C) Winter deployments. Right-hand panel is expanded view over sampling period. Discrete sample measurements shown as symbols; modeled unfiltered MeHg concentration time series shown as solid line; water depth shown as dashed line; precipitation shown as gray bars. Discrete samples were not collected during Winter in the side channel during the monitoring period.

per mass of sediment. Event-associated modeled concentrations were higher in the main channel than the side channel, suggesting the tide flats off the mouth of the main channel on the north side of the island were the source of the sediment. These high event-related modeled PMeHg concentrations occurred only during flood, with elevated concentrations in several ebb tides after these events, resulting in return of some of the storm-deposited material to the estuary (Fig. 8, Table 2).

However, there were systematic tidally related peaks in the PMeHg record distinctly different than those observed in the DMeHg time series. For example, in the Spring and Fall main channel time series, peaks in PMeHg concentration are associated with ebb tide, at the time of increasing MeHg concentrations and velocities in the tidal channels.

MeHg flux—The tidally coupled higher PMeHg concentration during ebb led to the unexpected result that particles dominate the MeHg flux on Browns Island. We hypothesized that off-island DMeHg fluxes would be greater than PMeHg fluxes because DMeHg concentrations are typically higher (Hill et al. 2009) and because the island is a net sink for sediment (Ganju et al. 2005). The modeled DMeHg fluxes were typically smaller than PMeHg fluxes because tidal exchange into surrounding river waters was comparatively low; wetland-derived DMeHg was transported up and down the channel, but smaller amounts were exchanged with surrounding river waters than for PMeHg. This effect is evident from the relative symmetry in the tidal peaks in DMeHg and was at least in part caused by the presence of a sill at the mouth of the main channel, which cut off the ebb flux: the highest dissolved concentrations were held on the island, limiting the flux (Fig. 3). It is interesting to note that winter was the season with the lowest DMeHg flux (Fig. 5), even though it had the highest DMeHg concentrations and largest difference in concentration between high and low tides (Fig. 3).

Nevertheless, the largest modeled single tide PMeHg fluxes were on-island (Fig. 5), associated with the high event-related particle concentrations that occurred during flood tides (Fig. 8), but these were countered by an off-island flux arising from the systematic elevation in PMeHg concentration that occurred on ebb tides. It was initially presumed that the elevated PMeHg concentrations on ebb were due to higher ebb velocities, but they were not associated with a concomitant increase in c_{p650}, an indicator of total particle concentration. This suggests that the higher MeHg loading on suspended sediments during

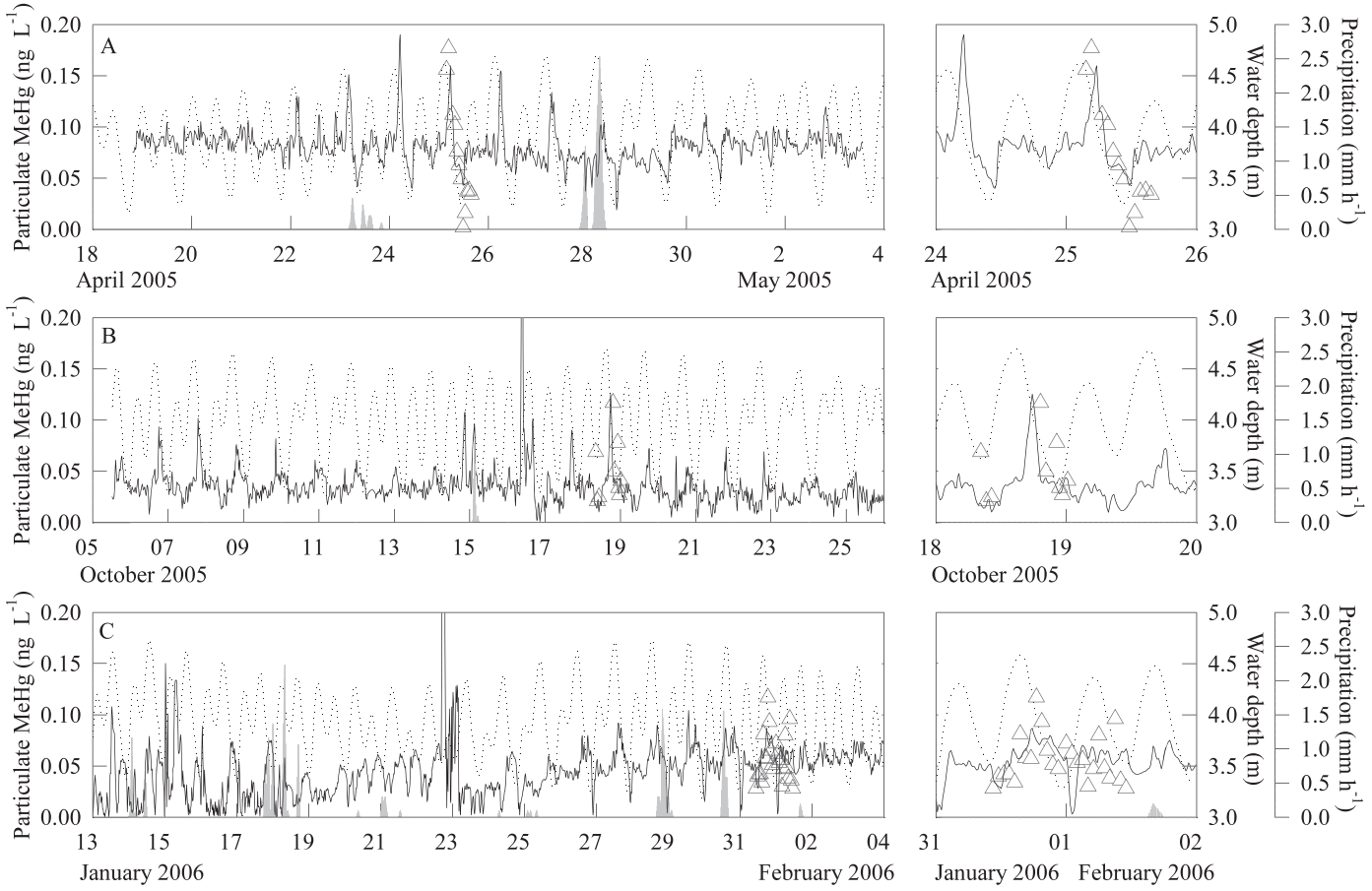

Fig. 8. Time series of particulate methylmercury in main channel site on Browns Island for (A) Spring, (B) Fall, and (C) Winter deployments. Right-hand panel is expanded view over sampling period. Discrete sample measurements shown as symbols; modeled particulate MeHg concentration time series shown as solid line; water depth shown as dashed line; precipitation shown as gray bars.

ebb lead to the flux, rather than higher suspended sediment concentrations. The slope of the particle spectra, S_{Cp}, was lower on ebb than on flood, indicating a larger particle size distribution on ebb, likely because of organic sorption or aggregation (Boss et al. 2001). These observations are consistent with a rapid partitioning of DMeHg onto suspended particles. Stronger relationships of PMeHg to POM on ebb than flood (Table 1) provides supporting evidence. These findings indicate how wetland interaction might act to increase particle loadings of MeHg, even if the particles are not deposited.

As a consequence of the dominance of the particulates, the unfiltered MeHg fluxes over single tides varied considerably both within and between seasons, ranging from a maximum on-island flux of 34 mg per tide in Winter to a maximum off-island flux of 18 mg in Spring (Fig. 5). The range of UMeHg fluxes per tide within seasons varied from 26 mg in Spring (8 mg on-island to 18 mg off-island) to 49 mg in Winter (34 mg on-island to 15 mg off-island). The intertidal and interseasonal differences were caused by differences in tides, storms, regional water levels, wetland geometry, and other factors, the combined effects of which are unpredictable, demonstrating that high-frequency monitoring techniques such as the one presented here are essential to adequately quantify fluxes.

The seasonality of both the wetland and regional concentrations and fluxes correspond with the regional concentrations of particulate and dissolved MeHg observed previously (Choe et al. 2003), as well as the seasonal changes in dissolved organic carbon (Kraus et al. 2008), suggesting similar processes are driving the local and regional variation, and highlighting the need for year-round assessments to better characterize tidal export.

MeHg yield—Although the concept of quantifying MeHg yields (flux per unit area) does not translate well to the site at Browns Island because the drained area varies by tide and by season, it is useful for rough comparison to other sites in the estuary and elsewhere. The annualized MeHg yield calculated on the basis of the discharge and tidal differential (*see* Methods) was 3.6, 2.2, and 1.7 μg m^{-2} yr^{-1} in Spring, Winter, and Fall, respectively, for an estimated annual yield of 2.5 μg m^{-2} yr^{-1}. The proportional difference in yield between seasons is smaller than for flux, suggesting the seasonal differences in MeHg production could be smaller than it might appear from the concentration or integrated flux values; export per unit area is similar throughout the year.

The MeHg yields estimated in this study are 4–40 times higher than the relatively few reported yields for terrestrial

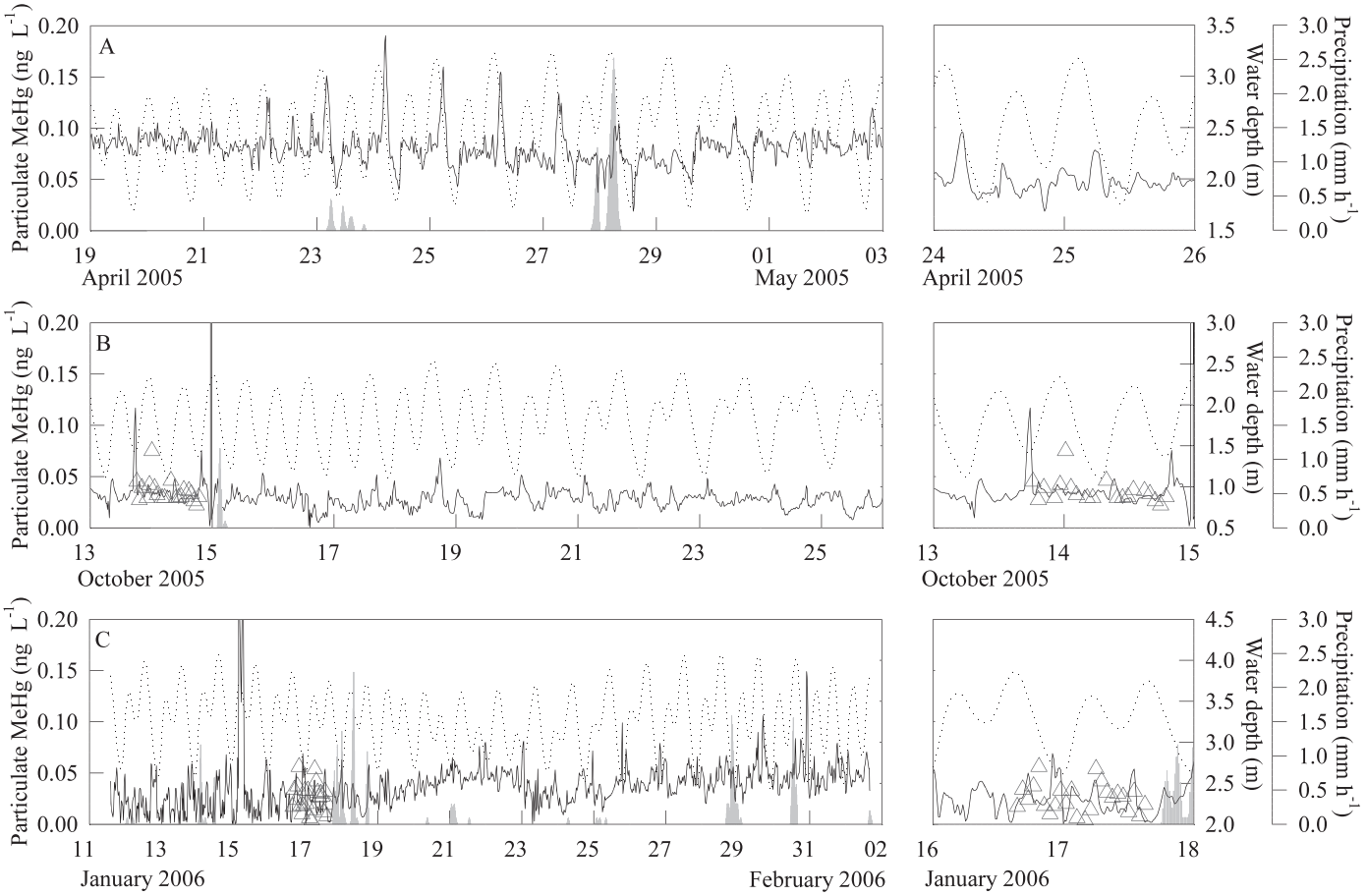

Fig. 9. Time series of particulate methylmercury in side channel site on Browns Island for (A) Spring, (B) Fall, and (C) Winter deployments. Right-hand panel is expanded view over sampling period. Discrete sample measurements shown as symbols; modeled particulate MeHg concentration time series shown as solid line; water depth shown as dashed line; precipitation shown as gray bars. Discrete samples were not collected during Winter in the side channel during the monitoring period.

wetland (St. Louis et al. 1994; Krabbenhoft et al. 1995; Hamilton et al. 2005), suggesting that tidal flushing has a large effect or that this type of marsh has inherently higher MeHg production rates. These results are within the broad range of yields reported for tidal wetlands in the San Francisco estuary on the basis of measurement of single tides (-14 to 5 μg m^{-2} yr^{-1}; Gill 2008) and similar to yields reported for two nontidal bulrush wetlands in the Sacramento delta (2.8 and 5.3 μg m^{-2} yr^{-1}; Sassone et al. 2008). It is much smaller than the yield used to calculate the estuary mass balance for California's MeHg total maximum daily load (TMDL) regulations (7 μg m^{-2} yr^{-1}; Wood et al. 2010).

If Browns Island represents the average tidal wetland, then the yield from 33.3 km^2 of tidal wetlands of the Sacramento–San Joaquin delta (Jassby and Cloern 2000) contributes roughly 80 g yr^{-1} MeHg to the San Francisco estuary, equivalent to 3% of the river-borne load (Wood et al. 2010). If the current plans to implement 240 km^2 of tidal wetland restoration in the estuary are achieved and the yields are similar to those reported here, the total load from tidal wetlands will represent more than 20% of the river load, or 700 g yr^{-1}. Furthermore, inundation models with moderate levels of future sea-level rise indicate up to 800 km^2 of land surrounding San Francisco will be below mean sea level (Knowles and Cayan 2002). In the unlikely event these lands all become tidal wetlands and existing wetlands keep pace with sea level rise, the total tidal wetland MeHg loading to the estuary could be in the range of 2 kg yr^{-1}, or roughly 70% of the current river loading.

Implications—The techniques developed for this study demonstrate the potential to relate biogeochemical processes to hydrodynamic and meteorological forcings in ways heretofore impossible because of the unpredictable, rapid, and sporadic nature of concentration change in dynamic systems. Combining high-frequency optical proxy measurements with physical ones has lead to substantial advances in the ability to understand and quantify sediment dynamics (Schoellhamer 2002; Ganju et al. 2005). Application of analogous measurements to chemical dynamics, as was done here, holds similar promise, although much work needs to be done to assess the extent to which relationships are specific to the site and conditions. High-frequency variation of chemical concentrations in the environment is an often-overlooked reality, but it provides important and newly accessible information about processes in the environment (Spencer et al. 2007; Pellerin et al. 2009).

The time series obtained by these techniques suggests, for example, that wetland geometries having a pronounced flood–ebb hysteresis—one that perches water on the marsh plain to drain through soil flow paths—might export more DMeHg than similar wetlands with freer exchange. These finding are contrary to the idea that minimizing the number of small sloughs within a restored wetland will lower DMeHg export. The situation is more complex—the particulars of how channels interact with the marsh plain are important. The ability to examine the time series data makes this obvious.

The suggestion from this data is also that relatively minor geomorphic features such as a sill that cuts off the ebb exchange will limit DMeHg export, but it is clear that resulting hydrodynamics must be considered; the presence of a sill can elevate channel velocities and thus lead to greater PMeHg exchange. A complete conceptualization of wetland biogeochemical, hydrodynamic, and geomorphic properties is essential in planning restorations that minimize MeHg export.

Finally, there are important implications for conduct of future studies in tidal systems. The overarching conclusion of the study was that complex interactions between physical features, tides, and random events, such as the timing of storms or wind events, combine in unpredictable ways to determine MeHg export. The results show the complex interplay between MeHg export and physical processes and demonstrate why better tools to assess flux are necessary. Our findings call into question whether existing monitoring programs or short-term studies are adequate for understanding sources, important influences, and fluxes. Longer term studies and studies that compare across several wetlands are imperative for a better understanding of the interactions between hydrodynamics and biogeochemistry in tidal wetland systems.

Acknowledgments

We thank the field and lab staff of the U.S. Geological Survey California Water Science Center and the California Department of Fish and Game Moss Landing Laboratory. In particular, we acknowledge the outstanding efforts of Megan Lionberger, Gail Wheeler, Erica Kalve, Will Kerlin, Matt Kerlin, Travis VonDessonneck, Brad Sullivan, Paul Buchanan, Connie Clapton, Autumn Bohnema, and Greg Brewster. We are grateful to Brian Branfireun, Jamie Shanley, David Krabbenhoft, Aria Amirbahman, and Gary Gill, whose comments and discussions have contributed to this work. We also thank two anonymous reviewers who helped improve the paper.

This work was supported by funding from the California Bay Delta Authority Ecosystem Restoration and Drinking Water Programs (grant ERP-00-G01) and matching funds from the U.S. Geological Survey Cooperative Research Program.

References

Bengtsson, G., and F. Picado. 2008. Mercury sorption to sediments: Dependence on grain size, dissolved organic carbon, and suspended bacteria. Chemosphere **73:** 526–531, doi:10.1016/j.chemosphere.2008.06.017

Benoit, J. M., D. H. Shull, R. M. Harvey, and S. A. Beal. 2009. Effect of bioirrigation on sediment–water exchange of methylmercury in Boston Harbor, Massachusetts. Environ. Sci. Technol. **43:** 3669–3674, doi:10.1021/es803552q

Bird, S. M., M. S. Fram, and K. L. Crepeau. 2003. Method of analysis by the U.S. Geological Survey California District Sacramento Laboratory—determination of dissolved organic carbon in water by high temperature catalytic oxidation, method validation, and quality-control practices [Internet]. Sacramento (CA): U.S. Geological Survey Open–File Report 03-366. Available from http://pubs.usgs.gov/of/2003/ofr03366/text.html.

Boelter, D. H. 1964. Water storage characteristics of several peats in situ. Proc. Soil Sci. Soc. Am. **28:** 433–435, doi:10.2136/sssaj1964.03615995002800030039x

Boss, E., W. S. Pegau, M. Lee, M. Twardowski, E. Shybanov, G. Korotaev, and F. Baratange. 2004. Particulate backscattering ratio at LEO 15 and its use to study particle composition and distribution. J. Geophys. Res.–Oceans **109:** C01014, doi:10.1029/2002JC001514

———, M. S. Twardowski, and S. Herring. 2001. Shape of the particulate beam attenuation spectrum and its inversion to obtain the shape of the particulate size distribution. Appl. Optics **40:** 4885–4893, doi:10.1364/AO.40.004885

California Data Exchange Center (CDEC). 2010. California Data Exchange Center. California Department of Water Resources [accessed 2010 December]. Available from http://cdec.water.ca.gov

Canario, J., C. Vale, and M. Nogueira. 2008. The pathway of mercury in contaminated waters determined by association with organic carbon (Tagus estuary, Portugal). Appl. Geochem. **23:** 519–528, doi:10.1016/j.apgeochem.2007.12.019

Choe, K. Y., G. A. Gill, and R. Lehman. 2003. Distribution of particulate, colloidal, and dissolved mercury in San Francisco Bay estuary. 1. Total mercury. Limnol. Oceanogr. **48:** 1535–1546, doi:10.4319/lo.2003.48.4.1535

———, ———, R. D. Lehman, S. Han, W. A. Heim, and K. H. Coale. 2004. Sediment–water exchange of total mercury and monomethyl mercury in the San Francisco Bay–Delta. Limnol. Oceanogr. **49:** 1512–1527, doi:10.4319/lo.2004.49.5.1512

Crump, K. L., and V. L. Trudeau. 2009. Mercury-induced reproductive impairment in fish. Environ. Toxicol. Chem. **28:** 895–907, doi:10.1897/08-151.1

Dittman, J. A., J. B. Shanley, C. T. Driscoll, G. R. Aiken, A. T. Chalmers, and J. E. Towse. 2009. Ultraviolet absorbance as a proxy for total dissolved mercury in streams. Environ. Pollut. **157:** 1953–1956, doi:10.1016/j.envpol.2009.01.031

Downing, B. D., B. A. Bergamaschi, D. G. Evans, and E. Boss. 2008. Assessing contribution of DOC from sediments to a drinking-water reservoir using optical profiling. Lake Reservoir Manag. **24:** 381–391, doi:10.1080/07438140809354848

———, E. Boss, B. A. Bergamaschi, J. A. Fleck, M. A. Lionberger, N. K. Ganju, D. H. Schoellhamer, and R. Fujii. 2009. Quantifying fluxes and characterizing compositional changes of dissolved organic matter in aquatic systems in situ using combined acoustic and optical measurements. Limnol. Oceanogr.: Methods **7:** 119–131, doi:10.4319/lom.2009.7.119

Eagles-Smith, C. A., and J. T. Ackerman. 2009. Rapid changes in small fish mercury concentrations in estuarine wetlands: Implications for wildlife risk and monitoring programs. Environ. Sci. Technol. **43:** 8658–8664, doi:10.1021/es901400c

Eckard, R. S., P. J. Hernes, B. A. Bergamaschi, R. Stepanauskas, and C. Kendall. 2007. Landscape scale controls on the vascular plant component of dissolved organic carbon across a freshwater delta. Geochim. Cosmochim. Acta **71:** 5968–5984, doi:10.1016/j.gca.2007.09.027

Fitzgerald, W. F., C. H. Lamborg, and C. R. Hammerschmidt. 2007. Marine biogeochemical cycling of mercury. Chem. Rev. **107:** 641–662, doi:10.1021/cr050353m

Fleck, J. A., M. S. Fram, and R. Fujii. 2007. Organic carbon and disinfection byproduct precursor loads from a constructed, non-tidal wetland in California's Sacramento-San Joaquin Delta. San Francisco Estuary and Watershed Science **5:** 1–24.

Ganju, N. K., D. H. Schoellhamer, and B. A. Bergamaschi. 2005. Suspended sediment fluxes in a tidal wetland: Measurement, controlling factors, and error analysis. Estuaries **28:** 812–822, doi:10.1007/BF02696011

Gill, G. 2008. Task 4.2. Sediment–water exchange, p. 16. *In* Final Report submitted to the CALFED Bay–Delta Program for the project "Transport, cycling and fate of mercury and monomethylmercury in the San Francisco delta and tributaries." California Department of Fish and Game, Moss Landing Marine Laboratories, and Pacific Northwest National Laboratory.

Gorski, P. R., D. E. Armstrong, J. P. Hurley, and D. P. Krabbenhoft. 2008. Influence of natural dissolved organic carbon on the bioavailability of mercury to a freshwater alga. Environ. Pollut. **154:** 116–123, doi:10.1016/j.envpol.2007.12.004

Guentzel, J. L. 2009. Wetland influences on mercury transport and bioaccumulation in South Carolina. Sci. Total Environ. **407:** 1344–1353, doi:10.1016/j.scitotenv.2008.09.030

Hall, B. D., G. R. Aiken, D. P. Krabbenhoft, M. Marvin-Dipasquale, and C. M. Swarzenski. 2008. Wetlands as principal zones of methylmercury production in southern Louisiana and the Gulf of Mexico region. Environ. Pollut. **154:** 124–134, doi:10.1016/j.envpol.2007.12.017

Hamilton, S. K., S. J. Sippel, and S. E. Bunn. 2005. Separation of algae from detritus for stable isotope or ecological stoichiometry studies using density fractionation in colloidal silica. Limnol. Oceanogr.: Methods **3:** 149–157, doi:10.4319/lom.2005.3.149

Hammerschmidt, C. R., and W. F. Fitzgerald. 2006. Bioaccumulation and trophic transfer of methylmercury in Long Island Sound. Arch. Environ. Contam. Toxicol. **51:** 416–424, doi:10.1007/s00244-005-0265-7

Han, S., A. Obraztsova, P. Pretto, D. D. Deheyn, J. Gieskes, and B. M. Tebo. 2008. Sulfide and iron control on mercury speciation in anoxic estuarine sediment slurries. Mar. Chem. **111:** 214–220, doi:10.1016/j.marchem.2008.05.002

Heim, W. A., K. H. Coale, M. Stephenson, K. Y. Choe, G. A. Gill, and C. Foe. 2007. Spatial and habitat-based variations in total and methyl mercury concentrations in surficial sediments in the San Francisco Bay–Delta. Environ. Sci. Technol. **41:** 3501–3507, doi:10.1021/es0626483

Hill, J. R., N. J. O'Driscoll, and D. R. S. Lean. 2009. Size distribution of methylmercury associated with particulate and dissolved organic matter in freshwaters. Sci. Total Environ. **408:** 408–414, doi:10.1016/j.scitotenv.2009.09.030

Jassby, A. D., and J. E. Cloern. 2000. Organic matter sources and rehabilitation of the Sacramento-San Joaquin Delta (California, USA). Aquatic Conservation: Marine and Freshwater Ecosystems **10:** 323–352, doi:10.1002/1099-0755(200009/10)10:5<323::AID-AQC417>3.0.CO;2-J

Knowles, N., and D. R. Cayan. 2002. Potential effects of global warming on the Sacramento/San Joaquin watershed and the San Francisco estuary. Geophys. Res. Lett. **29:** 91–94, doi:10.1029/2001GL014339

Krabbenhoft, D. P., J. M. Benoit, C. L. Babiarz, J. P. Hurley, and A. W. Andren. 1995. Mercury cycling in the Allequash Creek watershed, northern Wisconsin. Water Air Soil Pollut. **80:** 425–433, doi:10.1007/BF01189692

Kraus, T. E. C., and others. 2008. Assessing the contribution of wetlands and subsided islands to dissolved organic matter and disinfection byproduct precursors in the Sacramento–San Joaquin River delta: A geochemical approach. Org. Geochem. **39:** 1302–1318, doi:10.1016/j.orggeochem.2008.05.012

Marvin-Dipasquale, M., J. Agee, C. McGowan, R. S. Oremland, M. Thomas, D. Krabbenhoft, and C. C. Gilmour. 2000. Methyl-mercury degradation pathways: A comparison among three mercury-impacted ecosystems. Environ. Sci. Technol. **34:** 4908–4916, doi:10.1021/es0013125

Mason, R. P., E. H. Kim, J. Cornwell, and D. Heyes. 2006. An examination of the factors influencing the flux of mercury, methylmercury and other constituents from estuarine sediment. Mar. Chem. **102:** 96–110, doi:10.1016/j.marchem.2005.09.021

Mergler, D., H. A. Anderson, L. H. M. Chan, K. R. Mahaffey, M. Murray, M. Sakamoto, and A. H. Stern. 2007. Methylmercury exposure and health effects in humans: A worldwide concern. Ambio **36:** 3–11, doi:10.1579/0044-7447(2007)36[3:MEAHEI]2.0.CO;2

Merritt, K. A., and A. Amirbahman. 2009. Mercury methylation dynamics in estuarine and coastal marine environments—a critical review. Earth-Sci. Rev. **96:** 54–66, doi:10.1016/j.earscirev.2009.06.002

Mitchell, C. P. J., and C. C. Gilmour. 2008. Methylmercury production in a Chesapeake Bay salt marsh. J. Geophys. Res.—Biogeosci. **113:** G00C04, doi:10.1029/2008JG000765

Mitro, M. G., D. C. Evers, M. W. Meyer, and W. H. Piper. 2008. Common loon survival rates and mercury in New England and Wisconsin. J. Wildl. Manag. **72:** 665–673, doi:10.2193/2006-551

Pellerin, B. A., and others. 2009. Assessing the sources and magnitude of diurnal nitrate variability in the San Joaquin River (California) with an in situ optical nitrate sensor and dual nitrate isotopes. Freshw. Biol. **54:** 376–387, doi:10.1111/j.1365-2427.2008.02111.x

Puckett, H. M., and B. H. V. Buuren. 2000. Quality assurance project plan for the CALFED Project: "An assessment of ecological and human health impacts of mercury in the Bay–Delta watershed." California Department of Fish and Game.

Ravichandran, M. 2004. Interactions between mercury and dissolved organic matter—a review. Chemosphere **55:** 319–331, doi:10.1016/j.chemosphere.2003.11.011

Saraceno, J. F., B. A. Pellerin, B. D. Downing, E. Boss, P. A. M. Bachand, and B. A. Bergamaschi. 2009. High-frequency in situ optical measurements during a storm event: Assessing relationships between dissolved organic matter, sediment concentrations, and hydrologic processes. J. Geophys. Res.—Biogeosci. **114:** G00F09, doi:10.1029/2009JG000989

Sassone, E., A. Bonnema, M. H. Stephenson, A. Wesley, A. Newman, J. Fleck, and K. Coale. 2008. Task 5.3a. Methylmercury loading studies in delta wetlands: Twitchell Island, p. 13. *In* Final Report submitted to the CALFED Bay–Delta Program for the project "Transport, cycling and fate of mercury and monomethylmercury in the San Francisco Delta and Tributaries." California Department of Fish and Game, Moss Landing Marine Laboratories, and Pacific Northwest National Laboratory.

Schoellhamer, D. H. 2002. Variability of suspended-sediment concentration at tidal to annual time scales in San Francisco Bay, USA. Cont. Shelf Res. **22:** 1857–1866, doi:10.1016/S0278-4343(02)00042-0

Selin, N. E. 2009. Global biogeochemical cycling of mercury: A review. Ann. Rev. Environ. Res. **34:** 43–63, doi:10.1146/annurev.environ.051308.084314

Sellers, P., C. A. Kelly, J. W. M. Rudd, and A. R. Machutchon. 1996. Photodegradation of methylmercury in lakes. Nature **380:** 694–697, doi:10.1038/380694a0

Spencer, R. G. M., and others. 2007. Diurnal variability in riverine dissolved organic matter composition determined by in situ optical measurement in the San Joaquin River (California, USA). Hydrol. Process. **21:** 3181–3189, doi:10.1002/hyp.6887

St. Louis, V. L., J. W. M. Rudd, C. A. Kelly, K. G. Beaty, N. S. Bloom, and R. J. Flett. 1994. Importance of wetlands as sources of methylmercury to boreal forest ecosystems. Can. J. Fish. Aquat. Sci. **51:** 1065–1076, doi:10.1139/f94-106

Stepanauskas, R., M. A. Moran, B. A. Bergamasch, and J. T. Hollibaugh. 2005. Sources, bioavailabitity, and photoreactivity of dissolved organic carbon in the Sacramento–San Joaquin River delta. Biogeochemistry **74:** 131–149, doi:10.1007/s10533-004-3361-2

Tan, S. W., J. C. Meiller, and K. R. Mahaffey. 2009. The endocrine effects of mercury in humans and wildlife. Crit. Rev. Toxicol. **39:** 228–269, doi:10.1080/10408440802233259

Twardowski, M. S., E. Boss, J. M. Sullivan, and P. L. Donaghay. 2004. Modeling the spectral shape of absorption by chromophoric dissolved organic matter. Mar. Chem. **89:** 69–88, doi:10.1016/j.marchem.2004.02.008

U.S. Environmental Protection Agency (EPA). 1996. Method 1669: Sampling ambient water for trace metals at EPA water quality criteria levels. U.S. Environmental Protection Agency Office of Water.

———. 1998. Method 1630: Methyl mercury in water by distillation, aqueous ethylation, purge and trap, and cold vapor atomic fluorescence spectrometry. U.S. Environmental Protection Agency Office of Water.

Weiss, R., J. Alm, R. Laiho, and J. Laine. 1998. Modeling moisture retention in peat soils. Soil Sci. Soc. Am. J. **62:** 305–313, doi:10.2136/sssaj1998.03615995006200020002x

Whalin, L., E. H. Kim, and R. Mason. 2007. Factors influencing the oxidation, reduction, methylation and demethylation of mercury species in coastal waters. Mar. Chem. **107:** 278–294, doi:10.1016/j.marchem.2007.04.002

Windham-Myers, L., and others. 2009. Experimental removal of wetland emergent vegetation leads to decreased methylmercury production in surface sediment. J. Geophys. Res.—Biogeosci. **114:** G00C05, doi:10.1029/2008JG000815

Wood, M. L., C. G. Foe, J. Cooke, and S. J. Louie. 2010. Sacramento–San Joaquin delta estuary TMDL for methylmercury, p. 376. Staff Report. California Environmental Protection Agency, Regional Water Quality Control Board, Central Valley Region.

Associate editor: Robert E. Hecky

Received: 03 December 2010
Accepted: 22 March 2011
Amended: 05 April 2011